JOURNAL OF Applied Polymer SCIENCE

Growth of silver nanowires on carbon fiber to produce hybrid/waterborne polyurethane composites with improved electrical properties

Xiaoyun An, Jingjing Ma, Kai Wang, Maosheng Zhan
School of Materials Science and Engineering, Beihang University, Beijing 100191, People's Republic of China
Correspondence to: M. Zhan (E-mail: zhanms@buaa.edu.cn)

ABSTRACT: One dimensional silver nanowires (AgNWs) were grown on carbon fiber (CF) by a facile polyol method. Fourier transform infrared spectrometer (FTIR), laser Raman spectrometer (Raman), field-emission scanning electron microscopy (FESEM), X ray diffraction instrument (XRD), energy dispersive spectrometer (EDS), and X-ray photoelectron spectrometer (XPS) were carried out to reveal the structure, morphology, and formation mechanism of the CF-AgNWs. It was found that $AgNO_3$ concentration of 1.5 m*M*, reaction temperature of 160°C, and reaction time of 120 min were appropriate conditions for growth of AgNWs on CF. Moreover, a mechanism was suggested that the cysteamine on CF acted as nucleation centers for growth of silver nanoparticles and then small sized silver nanoparticles reduced from silver nitrate were grown on CF via the silver bonding to sulfur. Through an Ostwald ripening process, small sized silver nanoparticles were grown into larger particles. With the assistance of polyvinylpyrolidone (PVP), these larger particles were directed to grow in a definite direction to form nanowires. It was found that the resistance of CF-AgNWs was decreased to 19.5 Ω, compared with that of CF (102.6 Ω) with the same quality. Thus, the CF-AgNWs was added into waterborne polyurethane (WPU) to improve the electrical and dielectric properties of WPU. Results showed the WPU/CF-AgNWs composite presented a lower percolation threshold than WPU/CF composite. When the content was 2.5 wt %, the volume resistivity of the WPU/CF-AgNWs (1.90×10^4 Ω cm^{-1}) was lower by approximately three orders of magnitude than that of WPU/CF (4.19×10^7 Ω cm^{-1}). When the content was 2.5 wt %, the dielectric constant and dielectric loss of the WPU/CF-AgNWs were improved to 15.24 and 0.21, which were 34.5 and 40.8% higher than that of WPU/CF. © 2015 Wiley Periodicals, Inc. J. Appl. Polym. Sci. **2016**, *133*, 43056.

KEYWORDS: composites; fibers; nanoparticles; nanowires and nanocrystals

Received 16 July 2015; accepted 15 October 2015
DOI: 10.1002/app.43056

INTRODUCTION

One dimensional (1D) silver nanowires (AgNWs) were promising nanomaterials due to their unique size-dependent optical properties,[1–3] dominant electrical conductivity,[4–6] and thermal properties.[7] It have been attractive for vast applications in nanoscale electronic devices,[8,9] such as Raman scattering (SERS),[10] biological sensors,[11,12] and transparent conducting electrodes.[13–16] Recently, significant interest has been directed toward the design of AgNWs composite in order to extend their range of applications.[17,18] In this case, carbon systems such as multi-walled carbon nanotubes and graphene have been composited with AgNWs to improve the electrical properties of the carbon systems.[19–22] For example, Samantara *et al.*[12] synthesized reduced graphene oxide (rGO)/AgNWs nanocomposite by dropping rGO to the system of AgNWs. The turn on field required to draw an emission current density of 1 μA cm^{-2} for the rGO–AgNWs (2.40 V mm^{-1}) was lower than that of the AgNWs (5.00 V mm^{-1}) and rGO (3.92 V mm^{-1}). Hsiao *et al.*[23] deposited AgNWs, which were modified with thiophenol, on graphene nanosheets (GNs) films to produce GNs/AgNWs hybrid nanomaterial films. The GN/AgNWs hybrid nanomaterial films exhibited a sheet resistance of 71 Ω sq^{-1}. Tien *et al.*[24] prepared graphene nanosheet (GN)/AgNWs hybrid nanomaterials. AgNWs, modified by cysteamine, were directly grafted on the surface of graphene oxide (GO) and then GO was reduced to GN. The AgNWs–GN hybrid nanomaterial films showed a sheet resistance of 86 Ω sq^{-1}. According to the above researches, AgNWs were produced first and then grafted on other carbon systems. So in order to simplify the preparation process, Cui *et al.*[25] fabricated a novel composite which was constructed by *in situ* growth of AgNWs on multi-walled carbon nanotubes (MWCNT) via the polyol method. The reduced platinum (Pt) nanoparticles were attached to the thioglycolic-treated MWCNT via Pt bonding to sulfur to act as the seeds for

Table I. Detailed Conditions of all Experiments in this Study

Sample	$AgNO_3$ concentration (m*M*)	Temperature (°C)	Time (min)
C1	3.0	160	120
C2	1.5	160	120
C3	0.75	160	120
C4	0.5	160	120
T1	1.5	140	120
T2	1.5	150	120
T3	1.5	160	120
T4	1.5	170	120
t1	1.5	160	15
t2	1.5	160	30
t3	1.5	160	60
t4	1.5	160	120

Notice: *C2*, *T3*, and *t4* are the same sample; *C* represents the concentration, *T* represents the temperature, *t* represents the time.

AgNWs and then MWCNT/AgNWs composite was produced. The MWCNT/AgNWs nanomaterial films exhibited a sheet resistance of 47.8 Ω sq^{-1}. From the above results, we concluded that grafting the AgNWs on carbon system could improve electrical properties. However, the carbon systems were all MWCNT and GN from the above researches. Thus, CF was selected instead of MWCNT and GN to prepare CF-AgNWs in terms of cost. To the best of our knowledge, there was still no literature reporting a preparation system about CF-AgNWs. Furthermore, the preparation process in the above research was complex and it could be simplified by directly growing AgNWs on CF without other metal nanoparticles.

Recently, there were some researches about growing nanowires on CF. But to the best of our knowledge, there was still no research about growing AgNWs on CF. Jun *et al.*[26] prepared cupric oxide-nanowire-covered carbon fibers by annealing the copper-coated carbon fiber (Cu/CF) in air. However, the annealing temperature was as high as 400°C, which was not safe and wasted much energy. Liao *et al.*[27] synthesized ZnO NWs/CF using the hydrothermal growth approach. The carbon fibers were covered with a seed of ZnO and then the ZnO NWs were grown on ZnO seed-coated carbon fibers via a hydrothermal method. The reaction condition was mild and it didn't need any after-treatment with high temperature. Furthermore, the AgNWs' conductivity was better than ZnO NWs'. Thus CF-AgNWs could be as fillers to greatly improve polymers' electrical property. In our research, the silver nanowires were directly grown on CF by a facile polyol method. The reaction conditions were also mild.

Waterborne polyurethane (WPU) with high electrical conductivity are critical for applications ranging from electrostatic automotive painting and electromagnetic shielding for mobile electronics.[28] However, WPU was an insulating material and its electrical property was poor, which limited the development of its application. To further improve the electrical properties of WPU, one of the most efficient methods was to add various kinds of fibers into the matrix. Kwon *et al.*[29] prepared a series of WPU/MWCNT composites by *in situ* polymerization. It was found that the electrical conductivity of the WPU/MWCNT containing 1.5 wt % CNTs (8.0×10^{-4} S cm^{-1}) were nearly eight orders of magnitude higher than that of WPU (2.5×10^{-12} S cm^{-1}). However CF was selected to fill into the WPU to improve the electrical properties in order to save costs. Lu *et al.*[30] used CF to reinforce polyurethane. At only 10 vol % of CF, the electrical conductivity was found to reach 10^{-8} S cm^{-1} at that CF content. Above all, although the addition of CF was helpful for saving costs, the electrical properties of WPU/CF was poor. Thus, CF-AgNWs was prepared instead of CF. CF-AgNWs was more easily to form conductive network due to the high aspect ratio of AgNWs. So it could enhance the electrical properties of composites with a low content. In conclusion, it may help achieve not only cost savings, but also desirable electrical property.

Herein, the CF-AgNWs was prepared by a simple and straightforward synthetic route and its structure, morphology, and formation mechanism were studied. To optimize process, a systematic study was carried out including the effect of the $AgNO_3$ concentration, reaction temperature and reaction time

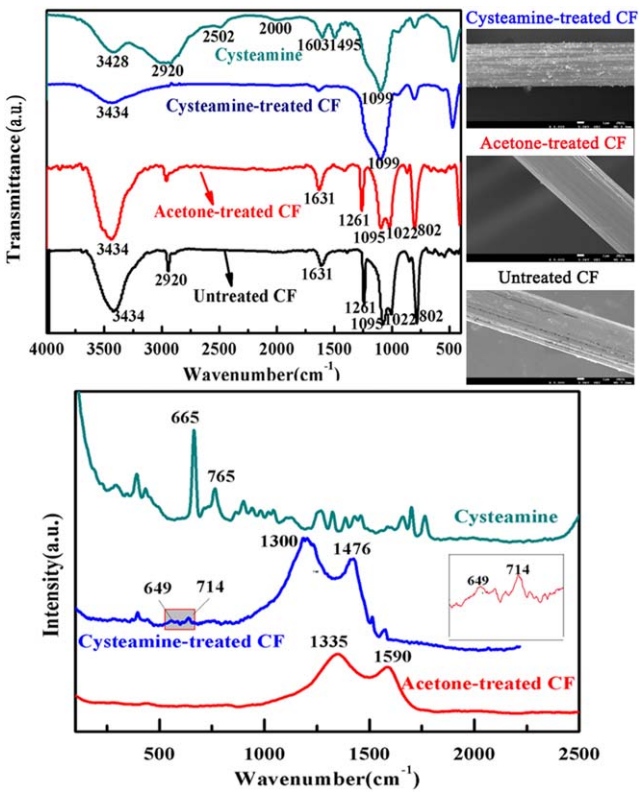

Figure 1. (a) FTIR spectra of cysteamine, untreated CF, acetone-treated CF and cysteamine-treated CF. (b) Raman spectra of cysteamine, acetone-treated CF and cysteamine-treated CF. Inset (a) shows the FESEM images of: untreated CF, acetone-treated CF and cysteamine-treated CF. [Color figure can be viewed in the online issue, which is available at wileyonlinelibrary.com.]

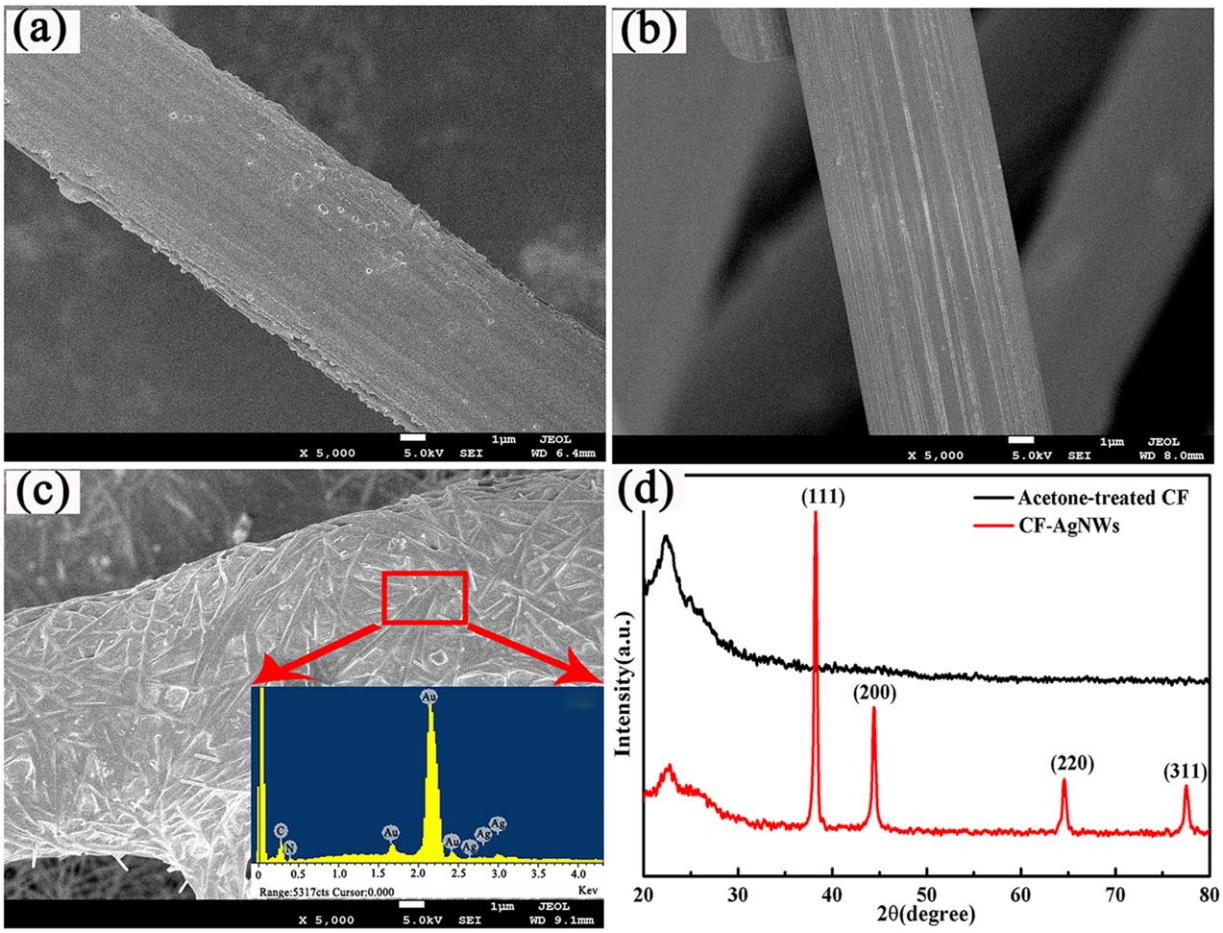

Figure 2. FESEM images of growth of AgNWs on: (a) untreated CF, (b) acetone-treated CF, (c) cysteamine-treated CF. Inset (c) shows the EDS of the selected area of the sample. (d) XRD pattern of acetone-treated CF and the CF-AgNWs. [Color figure can be viewed in the online issue, which is available at wileyonlinelibrary.com.]

on morphology of CF-AgNWs. Formation mechanism of growth of AgNWs on CF was further discussed. The CF-AgNWs was filled into WPU to improve the electrical properties. Moreover, the electrical properties, dielectric properties and mechanical properties of WPU filled with CF-AgNWs were investigated. CF-AgNWs could be as a filler to improve the materials' electrical property and was a potential candidate for EMI shielding applications.

EXPERIMENTAL

Materials

CF (T700) was purchased from Yancheng Ailiwei Fiber, China. $AgNO_3$ (≥99.0% purity), NaCl (≥99.5% purity), cysteamine (≥99.0% purity), ethanol, acetone, and deionized water were all supplied by Beijing Finechem, China. Ethylene glycol (EG) (≥99.5% purity) and PVP ($M_w \approx 40{,}000$, ≥99.0% purity) were purchased from Xilong Chemical Industry Incorporated, China. WPU were purchased from Beijing Shengshi, China. All chemicals were of analytical grade and used without further purification.

Surface Treatment of CF

The CF was treated with cysteamine according to the previous study.[24] CF was cut into 2 mm first and then Soxhlet extracted with acetone for 20 h. Next, CF (20 mg), cysteamine (71.2 mg) and RO water (40 mL) were added to a 250 mL volume flask and stirred at room temperature for 24 h. Then, the suspension was washed properly with DI water and centrifuged two times at 6000 rpm to separate CF from the suspension. The separated CF was dried immediately at 100°C for 1 h and 120°C for 2 h, and then stored for future use.

Preparation of CF-AgNWs

The CF-AgNWs was synthesized following a polyol method according to previous study.[31] In a typical procedure, 10 mg cysteamine-treated CF and 34 mL 6.0 m*M* PVP solution in EG were added to a 250-mL flask and stirred at room temperature for 1 h. Then the mixture was heated to 160°C by oil bath heating until the temperature was steady. Afterward, 40 μL of a 0.75 m*M* NaCl solution in EG was injected into the heated flask. After 5 min, 6 mL 3.0 m*M* $AgNO_3$ solution in EG was added into the dropping funnel and then added dropwise into the flask. $AgNO_3$ solution in EG was dripping slowly until the

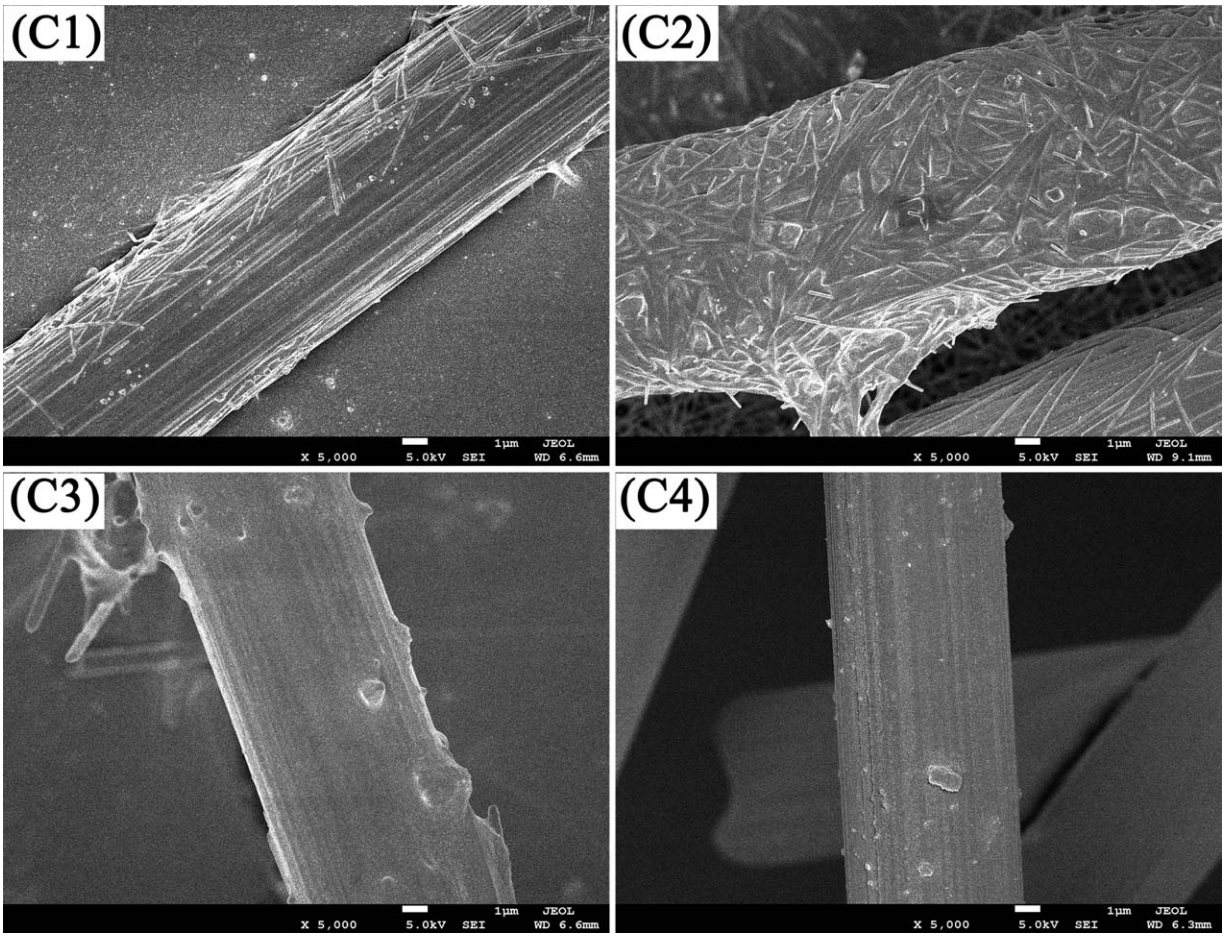

Figure 3. FESEM images of the CF-AgNWs with different $AgNO_3$ concentrations: (*C*1) 3.0 m*M*, (*C*2) 1.5 m*M*, (*C*3) 0.75 m*M*, (*C*4) 0.5 m*M*.

solution became purple, then all of the remaining $AgNO_3$ solution was added into the flask at once. The ratio of $AgNO_3$ to PVP was constant. Then obtained mixture was stirred at 160°C for 2 h and cooled down to room temperature naturally, then the suspension was centrifuged with ethanol three times at 6000 rpm for 20 min. The CF-AgNWs sample was dispersed in ethanol and stored for future use.

To investigate the effect of $AgNO_3$ concentration, reaction temperature, and reaction time on the morphology of CF-AgNWs, a series of samples were prepared as shown in Table I.

Preparation of WPU/CF-AgNWs Composites

The pristine CF and CF-AgNWs were respectively added into the WPU and stirred until homogenously distribution. The resulting composite was further cured under vacuum at 40°C, 5 h. A series of WPU/CF composites were prepared with the CF loadings varied between 0.5 and 2.5 wt %. These samples were expressed as WPU/CF0.5, WPU/CF1.0, WPU/CF1.5, WPU/CF2.0, and WPU/CF2.5 whose contents of CF were 0.5, 1.0, 1.5, 2.0, and 2.5 wt %, respectively. For comparison studies, the same content of CF-AgNWs was filled in the WPU. These samples were expressed as WPU/CF-AgNWs0.5, WPU/CF-AgNWs1.0, WPU/CF-AgNWs1.5, WPU/CF-AgNWs2.0, and WPU/CF-AgNWs2.5, respectively.

Characterization

Fourier-transform infrared spectroscopy (FTIR) was obtained on a Nexus-470 spectrometer with a spectral resolution of 6 cm^{-1} in the scan range from 400 to 4000 cm^{-1} to characterize the structures of the products. Laser Raman spectra (HR 800UV) were recorded from 100 to 2500 cm^{-1} with the laser wavelength of 633 nm to characterize the structures of the products. Field-emission scanning electron microscopy (FESEM, JSM 7500) was used to characterize the morphologies of the products at an accelerating voltage of 5 kV. Energy dispersive spectrometer (EDS) coupled to Field-emission scanning electron microscopy (FESEM) was used to analyze the composition of samples. X-ray diffraction instrument (XRD, D/max 2200 PC) was operated at a voltage of 40 kV and a current of 40 mA with Cu Kα radiation ($\lambda = 0.15406$ nm) with a scanning rate of 0.02° s^{-1} ranging from 20° to 80°. X-ray photoelectron spectroscopy (XPS, ESCALAB 250) was carried out using a monochromatized Al Kα X-ray source at a constant rate with 200 eV for survey and 30 eV for high resolution scans. The volume resistivity of WPU/CF composite and WPU/CF-AgNWs composite were measured using a digital multimeter (mastech ms8217). The dielectric properties were measured with an impedance analyzer (Agilent 4991A) in the frequency range of 10^6 to 10^7 Hz. Tensile properties were conducted on the universal testing machine (HY-0350) with a stretching rate of 2

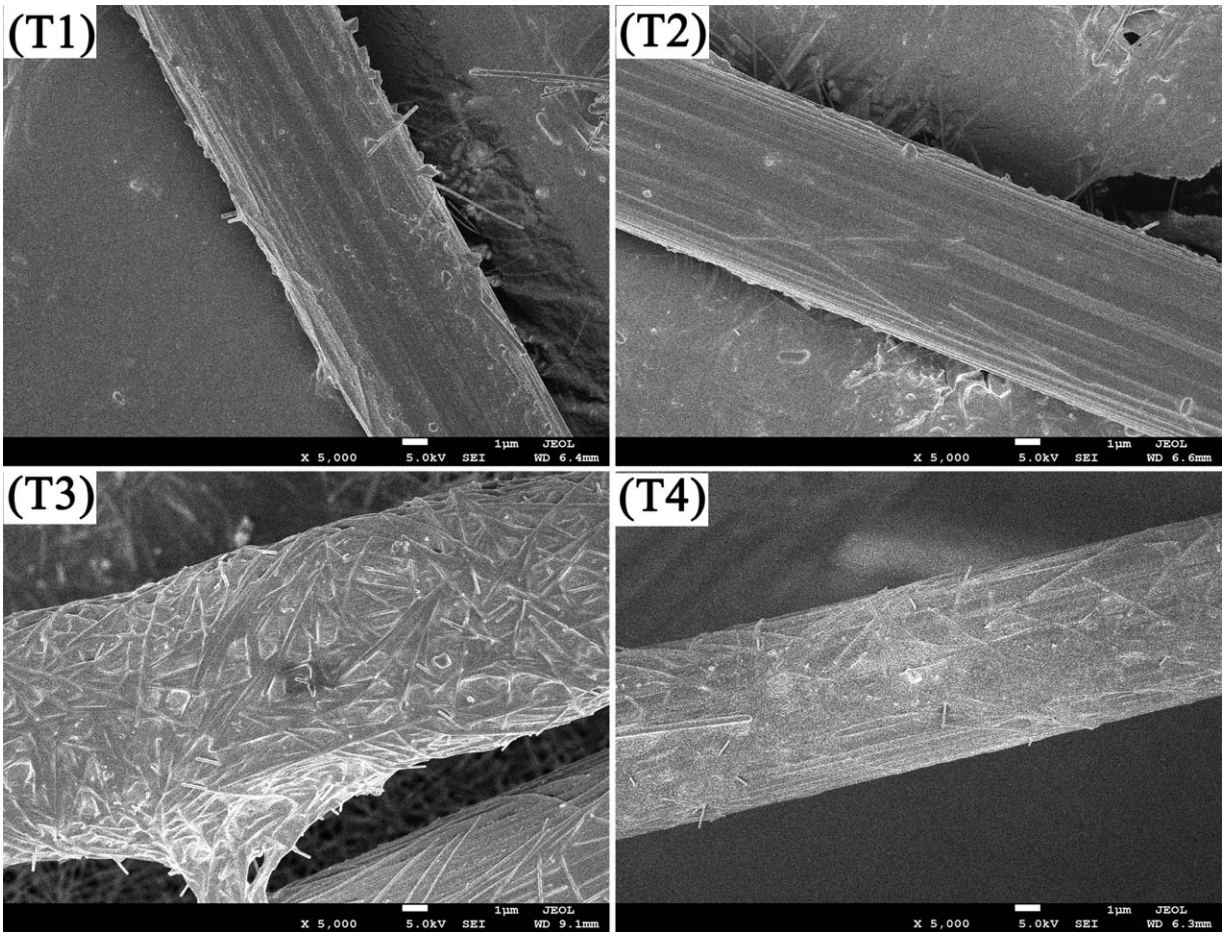

Figure 4. FESEM images of the CF-AgNWs with different reaction temperatures: (*T*1) 140°C, (*T*2) 150°C, (*T*3) 160°C, (*T*4) 170°C.

mm min^{-1}. The samples were cut into dumb-bell specimens for mechanical testing according to the Chinese national standard GB/T 1040-2006. The reported results were the averages with standard deviations of five tested samples for each composite.

RESULTS AND DISCUSSION

The Surface Treatment of CF

Figure 1(a) showed the FT-IR spectra of cysteamine, pristine CF, acetone-treated CF, and cysteamine-treated CF. The broad bands at 3434 cm^{-1} were assigned to the O—H stretching vibration of OH groups on the surface of CF.[32,33] The strong bands at 1631 cm^{-1} were attributed to the C═O stretching vibrations on the surface of CF.[34] The strong bands at 1261 and 802 cm^{-1} were attributed to the C—O—C stretching vibrations in epoxy group,[35,36] and the strong bands at 1095 and 1022 cm^{-1} were assigned to the C—O stretching vibrations.[37–39] These indicated that there was epoxy sizing agent on CF. As shown in FESEM images of untreated CF and acetone-treated CF, CF became smooth after treated by acetone. It indicated that impurities on CF were removed by acetone. From the FT-IR spectra of cysteamine, the strong bands at 3428 and 1603 cm^{-1} were assigned to the —NH stretching and bending vibrations.[40,41] The strong band at 2502 cm^{-1} was assigned to the —SH stretching vibration,[42–44] the strong bands at 2920 cm^{-1} was attributed to C—H stretching vibration[45,46] and a broad band at 1099 cm^{-1} was attributed to C—N stretching peak.[36] From the FT-IR spectra of cysteamine-treated CF, the strong bands at 3434 cm^{-1} was assigned to the O—H stretching vibration. However, because that —NH stretching vibrations was observed at 3428 cm^{-1}, the strong bands at 3434 cm^{-1} also was attributed to the —NH stretching vibrations. Compared the FT-IR spectrum pattern of cysteamine-treated CF with that of cysteamine, a broad C—N stretching vibration peak was observed at 1099 cm^{-1}. That may cover the peaks at 1261 and 802 cm^{-1}, which can't accurately indicate whether the epoxy groups on CF reacted with the amino groups of cysteamine or not. Also there was no stretching vibrations peak at 2502 cm^{-1}, it may be because the content was so low that —SH was not easy to be tested by FT-IR. Moreover, as FESEM image of cysteamine-treated CF showed, there were a layer of materials coated on CF. Therefore, in order to further characterize the chemical interaction between epoxy sizing agent and cysteamine, laser Raman spectroscopy was surveyed.

Furthermore, Raman analysis of the samples was carried out to verify the efficient reactions between epoxy sizing agent of CF and cysteamine [Figure 1(b)]. In the Raman spectra of acetone-treated CF, two prominent peaks appeared clearly at 1590 cm^{-1} (a tangential G-band) and 1335 cm^{-1} (a disorder-induced D-

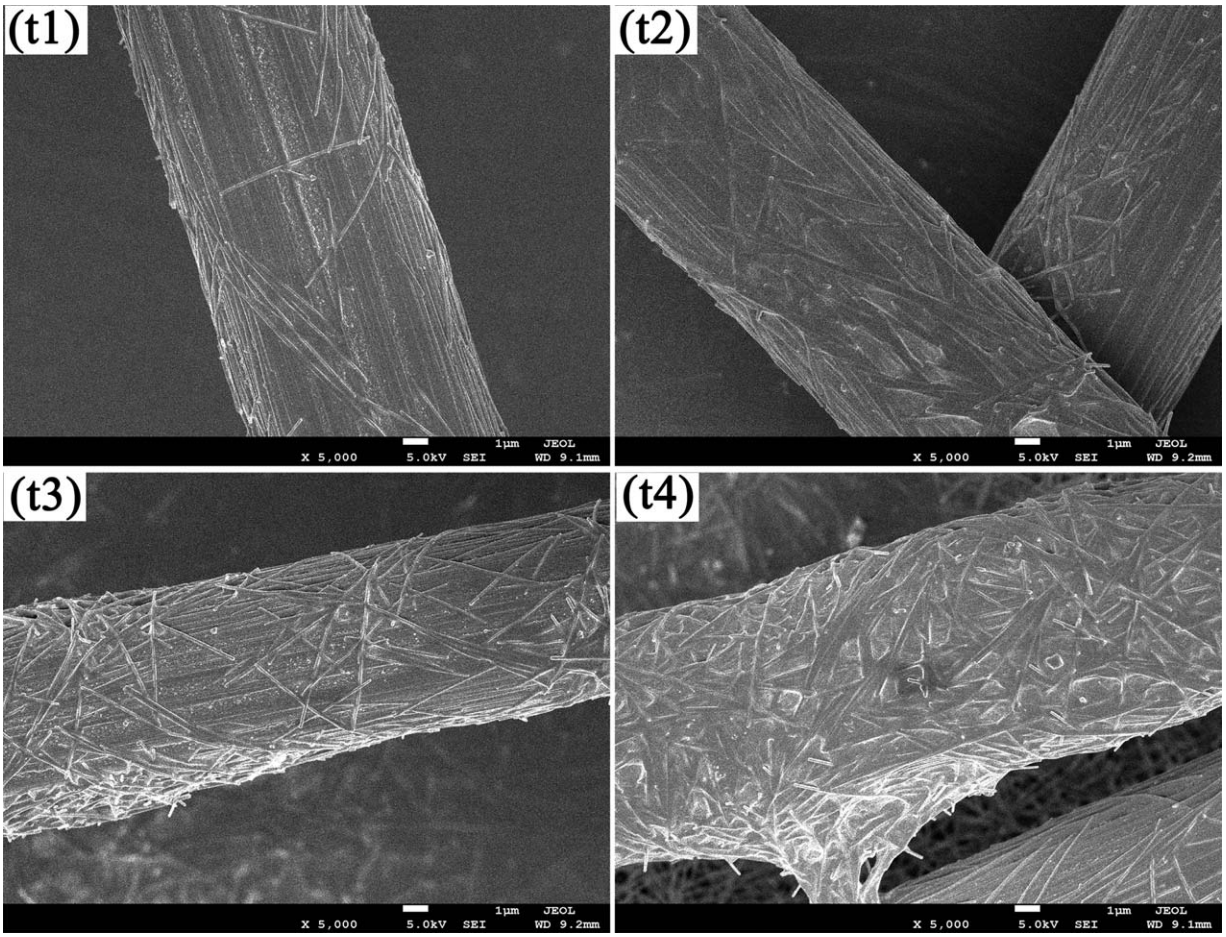

Figure 5. FESEM images of the CF-AgNWs with different reaction times: (*t*1) 15 min, (*t*2) 30 min, (*t*3) 60 min, (*t*4)120 min.

band). The G-band and D-band peaks of cysteamine-treated CF shifted to 1476 and 1300 cm^{-1}, suggesting the successful reaction between epoxy sizing agent of CF and cysteamine. The intensity ratio of the D and G bands (ID/IG) was found to be increased from acetone-treated CF (1.19) to cysteamine-treated CF (1.28), representing the successfully introduction of —NH. In the Raman spectra of cysteamine, the S—C peaks for *cis* conformers and *trans* conformers were seen at 665 and 765 cm^{-1} respectively.[47] By comparison, the S—C peak of the cysteamine-treated CF shifted to lower wavenumbers of 649 and 714 cm^{-1}, which related to a withdrawal of electron density from the C—S bond resulting from the bonding between the amino and the epoxy.

Characterization of CF-AgNWs

Effects of Different Surface Treatments. Figure 2 showed the effects of different surface treatments on the morphology of products. Figure 2(d) showed XRD patterns of acetone-treated CF and the CF-AgNWs. There were no AgNWs on untreated CF and acetone-treated CF [Figure 2(a,b)]. While AgNWs were grown on cysteamine-treated CF successfully as shown in Figure 2(c), which indicated that the cysteamine promoted the growth of Ag nanowires on the surface of CF. Furthermore, the presence of C and Ag in EDS spectra indicated that silver nanowire was on CF. XRD analysis of the samples was carried out to verify the formation of the CF-AgNWs [Figure 2(d)]. The acetone-treated CF and CF-AgNWs pattern both had a strong peak at 22.36° which corresponded to the C (002) reflection of a turbostratic carbon structure of CF.[48] The other four peaks at about 38.22°, 44.45°, 64.62°, and 77.57° for CF-AgNWs represented the (111), (200), (220), and (311) planes of face centered cubic Ag, respectively.[49] The intensity ratio of the (111) and (200) peaks was found to be 2.46 (the theoretical ratio was 2.5[50]), representing the enrichment of the (111) crystalline planes in the AgNWs. This observation further confirmed the growth of AgNWs on the CF.

Effect of $AgNO_3$ Concentration. FESEM images of CF-AgNWs with different $AgNO_3$ concentration of 3.0, 1.5, 0.75, and 0.5 m*M* were shown in Figure 3. As shown in Figure 3(C1,C2), AgNWs were grown on CF successfully and the most AgNWs were grown on CF with the $AgNO_3$ concentration of 1.5 m*M*. As the concentration of $AgNO_3$ was decreased to 0.75 and 0.5 m*M* [Figure 3(C3,C4)], no AgNWs was on CF. From the results, we speculated that with the decrease of $AgNO_3$ concentration, the concentration of PVP was decreased due to the constant ratio of $AgNO_3$ to PVP. Moreover, more part of PVP was coated on CF. So there were less PVP in solution. A low

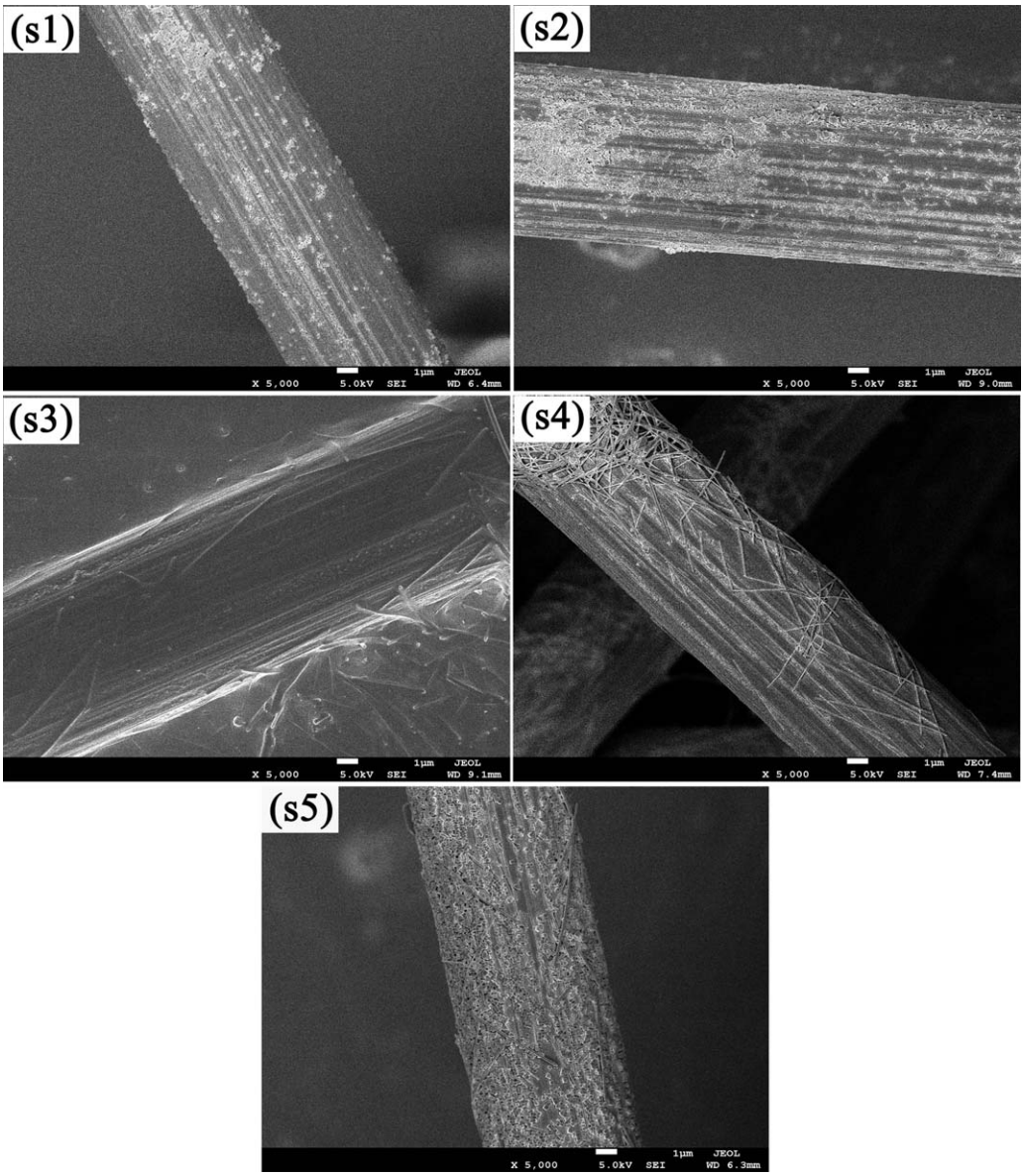

Figure 6. FESEM images of the CF-AgNWs synthesized with different feeding time: (*s*1) after slow dropping $AgNO_3$ (1×10^{-3} mol), (*s*2) after rapid dropping $AgNO_3$ (2×10^{-3} mol), (*s*3) reaction time for 3 min, (*s*4) reaction time for 10 min. (*s*5) FESEM image of cysteamine-treated CF mixing with AgNWs.

concentration of PVP caused larger seeds and insufficient passivation of the (100) facets, thus the growth along both (100) facets and (110) facets appeared, leading to nanorods with larger diameters.[31] Furthermore, there were silver nanoparticles appeared when the concentration of PVP decreased further. Thus, there were silver nanorods and silver nanoparticles with larger diameters grown on CF. However, the most AgNWs were grown on CF with $AgNO_3$ concentration of 1.5 m*M* not 3.0 m*M*. That because more PVP was packed on CF owing to the constant ratio of $AgNO_3$ to PVP which blocked silver bonding to sulfur. As shown in Figure 3(C1,C2), the length of AgNWs increased as the $AgNO_3$ concentration varied from 3.0 to 1.5 m*M*. This resulted from that the diameter and amount of silver seeds increased with the increase of $AgNO_3$ concentration. Meanwhile, the number of silver atoms for the growth of nanowires decreased leading to decreasing length.

Effect of the Reaction Temperature. FESEM images of the CF-AgNWs with different reaction temperatures of 140, 150, 160, and 170°C were shown in Figure 4. When the reaction temperature was as low as 140 and 150°C, AgNWs were hardly grown on CF [Figure 4(T1,T2)]. With the increase of temperature, AgNWs were grown on CF at 160 and 170°C. Moreover, a great deal of AgNWs was densely grown on CF with the temperature of 160°C. On the one hand, at low growth temperature (140 and 150°C), the nucleation of silver seeds was occurred in solution mainly, whereas at higher temperature, the silver seeds were grown on CF to act as nucleation center. On the other

hand, we speculated that as the growth temperature increased, self-diffusion of Ag atoms to the surface of CF became faster, contributing to formation of more nucleation centers on CF, leading to growth of AgNWs on CF. There were fewer AgNWs on CF at 170°C. It might because the chemical bonds that formed between amino of cysteamine and epoxy group of CF were destroyed or epoxy sizing agent was removed from CF, so less AgNWs were grown on CF.

Effect of Reaction Time. Figure 5 showed the FESEM images of the CF-AgNWs with different reaction times of 15, 30, 60, and 120 min. A small quantity of AgNWs was grown on CF as shown in Figure 5(t1). As the reaction time increased to 30 and 60 min, AgNWs grown on CF were increased gradually. However, AgNWs were not densely packed on CF as compared to that produced at a longer reaction time of 120 min [Figure 5(t4)]. We proposed that at the early of the reaction, the silver nitrate got reduced to form small sized silver nanoparticles, which reacted with cysteamine on CF, followed by the growth of larger particles through an Ostwald ripening process.[51–53] With the assistance of PVP, which controlled the growth rate of different faces of the silver by means of surface coordination, these larger particles were directed to grow in a definite direction to form nanowires. As the reaction continued, density of nucleation sites became larger so that the higher-density AgNWs were grown on CF. Finally a layer of AgNWs were grown on CF.

Analysis of Formation Mechanism of AgNWs on CF

To reveal the formation process of the AgNWs on the CF, we carried out time-dependent experiments during which samples were collected at different time intervals. Figure 6 showed the FESEM images of the products that were obtained at different growth stages. At the early stage, as $AgNO_3$ was dropped slowly, the surfaces of the CF became rougher and was covered by a great deal of small nanoparticles as shown in Figure 6(s1). The surface of the CF was not only covered by amount of small silver nanoparticles, but also a great deal of silver nanorods [Figure 6(s2)] with dropping $AgNO_3$ rapidly. As observed in Figure 6(s3), when the reaction time reached 3 min, AgNWs appeared, but the amount is very low. Prolonging the reaction time to 10 min, the surface of the CF was packed by more AgNWs [Figure 6(s4)]. From our experimental results, we proposed that the formation of AgNWs on the CF might be governed by formation of nucleation centers, growth of nucleus, followed by the well-known Ostwald ripening mechanism and growth of AgNWs. The evolution process was illustrated in Scheme 1. At the first stage, smaller silver nanoparticles that were reduced by EG, reacted fully with cysteamine to form nucleation centers. As the $AgNO_3$ was slowly dropped, the generated silver nanoparticles became larger, resulting in silver nanoparticle layer assembled on the surface of CF. Then as the $AgNO_3$ was rapidly dropped, some silver nanoparticles grown into silver nanorods with PVP that were absorbed on the surface of silver nanoparticles through Ag—O coordination. Because the surface energy of the (100) facets were higher than that of the (111) facets for silver seeds, the PVP molecules were tightly absorbed on the (100) planes according to the surface-energy minimization. That leaded to the rapid anisotropic

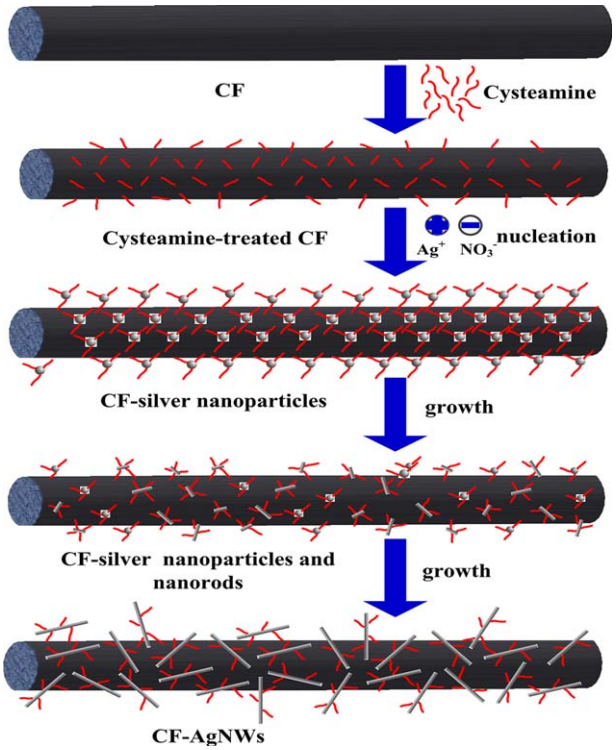

Scheme 1. Schematic illustration of the formation mechanism of AgNWs on CF.

growth along the (110) direction. Finally AgNWs were grown on the surface of CF. To prove that AgNWs were grown on CF, the studies of mixing AgNWs with cysteamine-treated CF were carried out. As shown in Figure 6(s5), the structure of AgNWs was destroyed, and sulfidized Ag nanoparticles were formed while attaching AgNWs on cysteamine-treated CF.

To further confirm the chemical composition and interaction of the prepared samples, the CF-AgNWs was further analyzed by XPS. As shown in Figure 7(a), peaks corresponding to C and O were both observed in the spectrum of cysteamine-treated CF and CF-AgNWs, which originated from the epoxy sizing agent on CF in consistent with the result of FTIR. Figure 7(b) showed the high resolution XPS spectrum for the C1s peak. The band located at 284.8 eV was assigned to the C—C bonds.[54] In addition, the bands centered at 285.2 and 285.6 ev were attributed to the C—S and C—N bonds,[55] which originated from cysteamine. Also, The bands located at 286.2, 286.9, and 287.9 ev were assigned to the C—O, C—O—C, and C═O bonds,[56] which were attributed to epoxy sizing agent on CF. This is also consistent with the result of FTIR. Figure 7(c) showed the high resolution XPS spectrum for the O1s peak. The bands centered at 531.9, 532.6, and 533.5 ev were attributed to the O—H, O—C, and O═C bonds,[52] which originated from epoxy sizing agent on CF. Furthermore, Figure 7(c) showed that percentage of O═C for cysteamine-treated CF (31.0%) was lower than that for CF-AgNWs (33.5%). It was due to the PVP molecules that were tightly absorbed on AgNWs. As shown in Figure 7(d), the splitting of the 3D doublet was 6.0 eV indicating the metallic

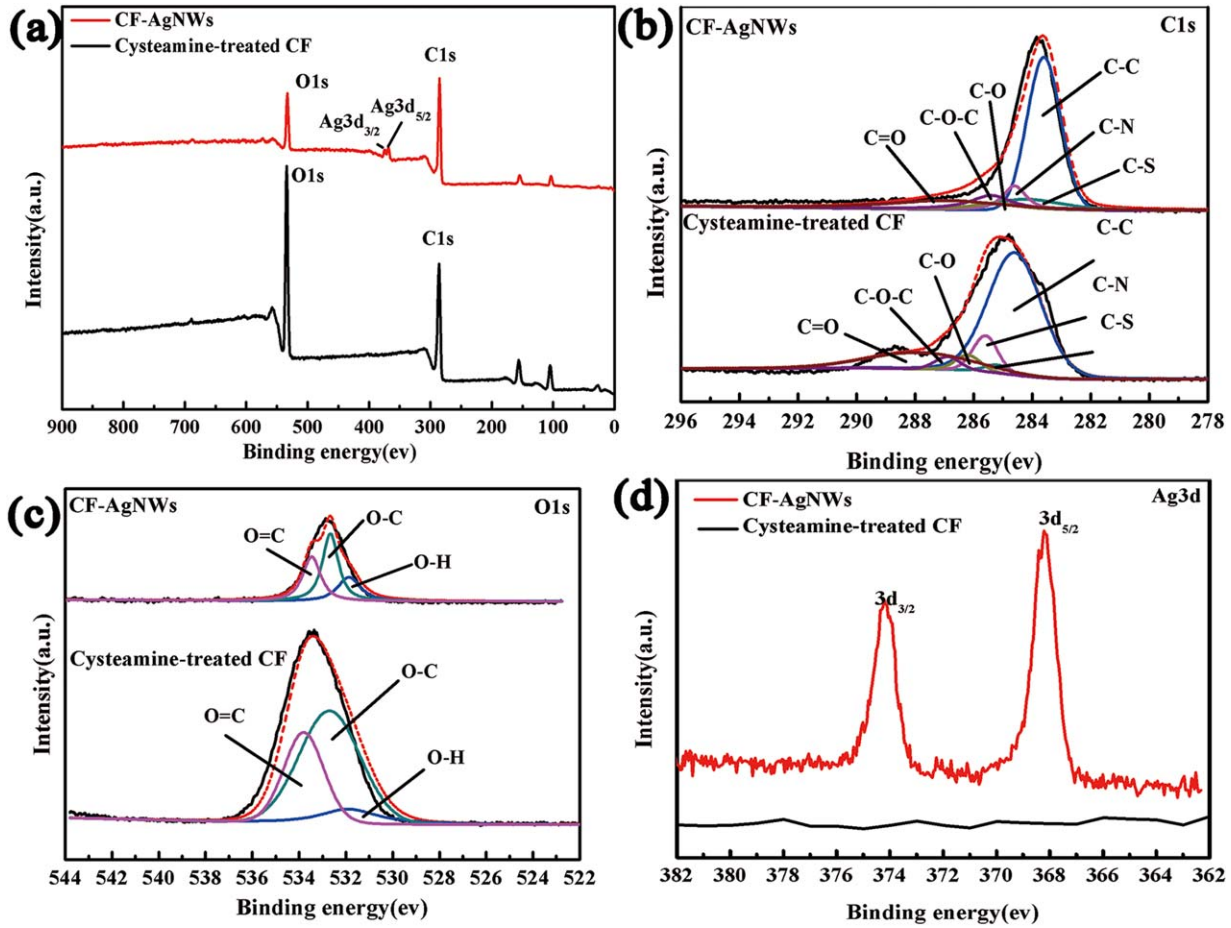

Figure 7. (a) XPS survey spectrum of cysteamine-treated CF and CF-AgNWs. XPS core level spectra of C1s (b), O1s (c), Ag3d (d) for cysteamine-treated CF and CF-AgNWs. [Color figure can be viewed in the online issue, which is available at wileyonlinelibrary.com.]

nature of silver. All of these confirmed that AgNWs were grown on the CF surface successfully.

Electrical Properties

The growth of AgNWs on CF could improve the electrical property of CF. It was found that the resistance of the CF-AgNWs was reduced to 19.5 Ω compared with that of the pristine CF with the same quality (102.6 Ω). Thus the CF-AgNWs could be as a filler to improve the electrical property of WPU. Figure 8 showed the volume resistivity of the WPU/CF composites and WPU/CF-AgNWs composites with different filler loadings. When the content of the pristine CF was ranged from 0 to 2.0 wt %, the volume resistivity of WPU/CF changed little and the WPU/CF composite was still insulator. However, the volume resistivity of WPU/CF composite was decreased significantly when the content of CF was 2.5 wt %. And the volume resistivity declined from 7.43×10^9 Ω cm^{-1}, for pure WPU, to 4.19×10^7 Ω cm^{-1} for the composite containing 2.5 wt % CF, suggesting that the composite was not insulated. As Figure 9(a–e) showed, CF could not achieve efficient touch due to the low content. But when the content of CF increased to 2.5 wt %, CF could contact with others partly as shown in Figure 9(f) and the connection of CF facilitates electrons transport along the CF and thereby the volume resistivity of WPU/CF composite changed evidently.

As Figure 8 showed, it was found that with the same loading, the volume resistivity of WPU/CF-AgNWs was lower than that

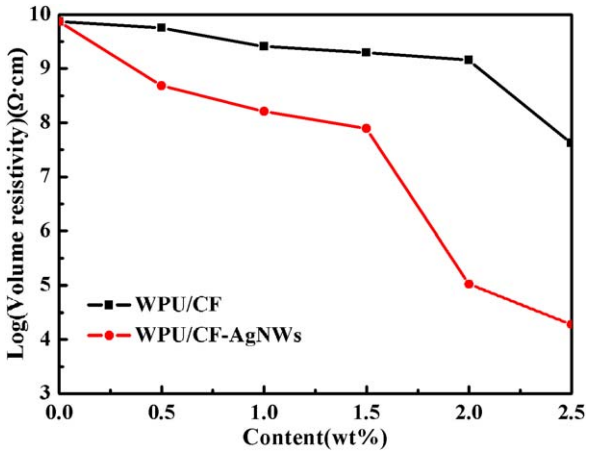

Figure 8. Volume resistivity of WPU/CF composites and WPU/CF-AgNWs composites with different filler contents. [Color figure can be viewed in the online issue, which is available at wileyonlinelibrary.com.]

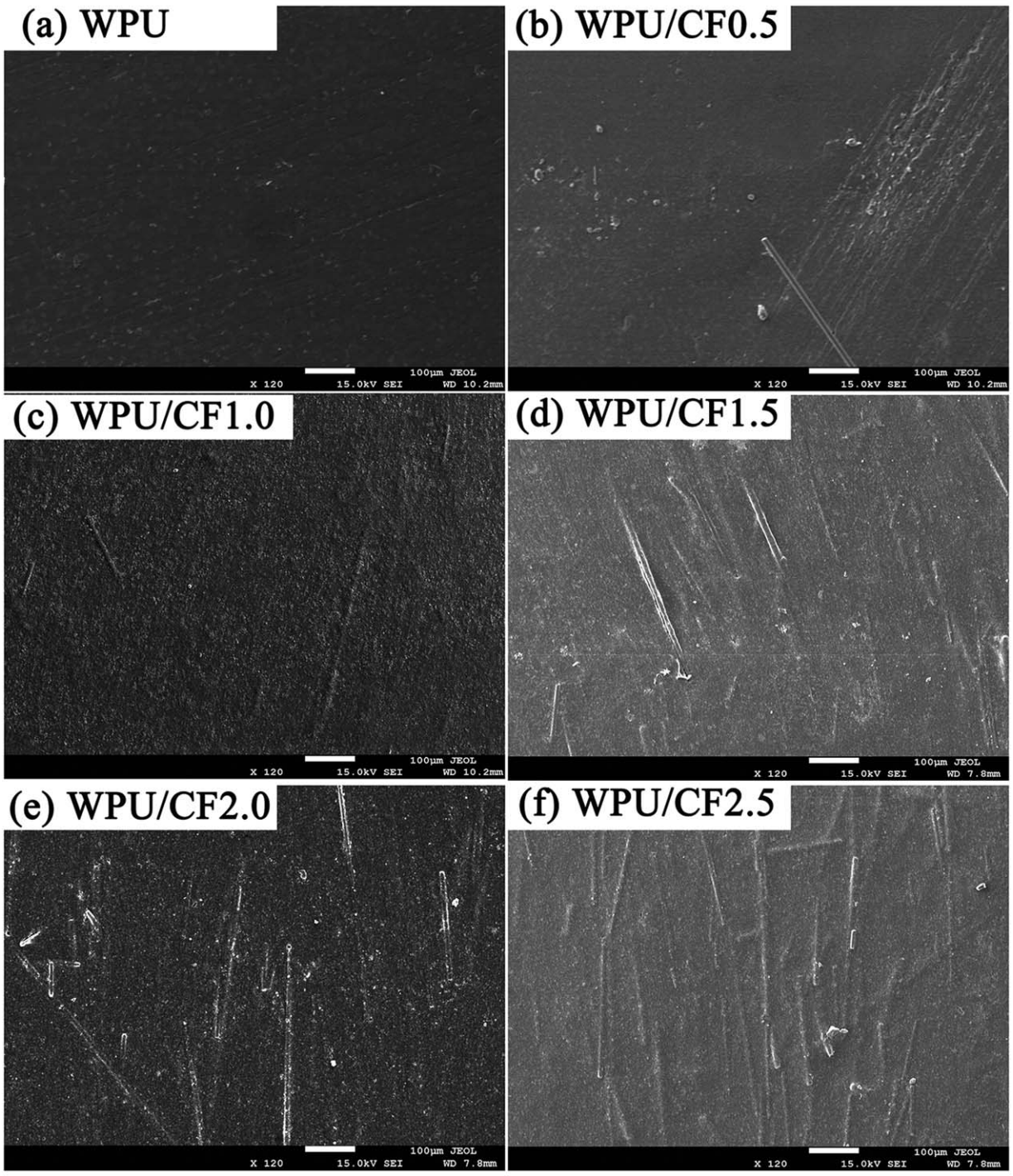

Figure 9. FESEM images of the net WPU (a) and WPU/CF composites with different contents of CF: 0.5 wt % (b), 1.0 wt % (c), 1.5 wt % (d), 2.0 wt % (e), and 2.5 wt % (f).

of WPU/CF. When the content of CF-AgNWs was ranged from 0 to 2.5 wt %, the volume resistivity of WPU/CF-AgNWs decreased with increasing content of CF-AgNWs. A zigzag drop in volume resistivity against the content of CF-AgNWs was observed. Specifically, the volume resistivity of WPU/CF-AgNWs decreased significantly to $1.06 \times 10^5\ \Omega\ cm^{-1}$ when the loading of CF-AgNWs was 2.0 wt %, which was lower by approximately three orders of magnitude than that of WPU/CF-AgNWs1.5. It was generally attributed to the percolation phenomenon. It was evident that the percolation threshold of the composites with CF and CF-AgNWs were very different. For the composite with CF, the percolation threshold values wasn't

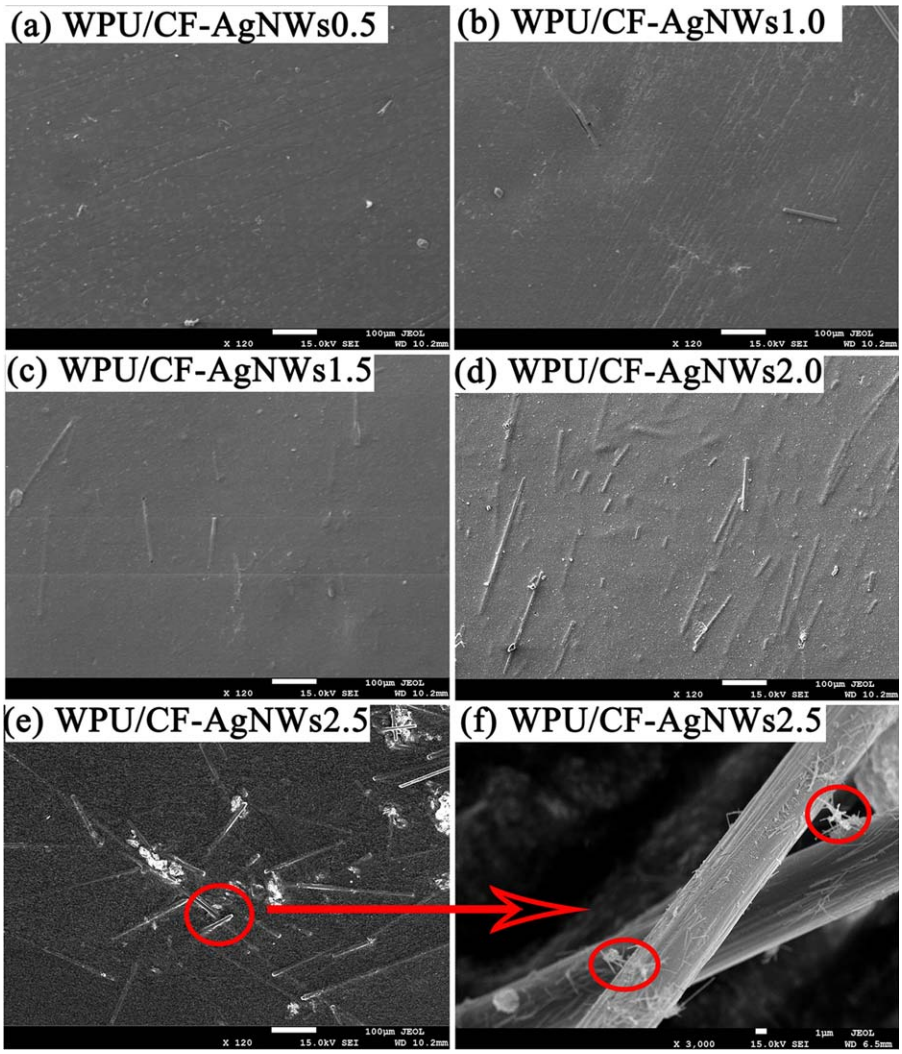

Figure 10. FESEM images of the WPU/CF-AgNWs composites with different contents of CF-AgNWs: 0.5 wt % (a), 1.0 wt % (b), 1.5 wt % (c), 2.0 wt % (d), and 2.5 wt % (e). (f) High multiple FESEM images of WPU/CF-AgNWs2.5. [Color figure can be viewed in the online issue, which is available at wileyonlinelibrary.com.]

observed when the content was ranged from 0 to 2.5 wt % and the higher percolation threshold values could be observed. Therefore, as a comparison with the WPU/CF-AgNWs composite, the higher concentrations of CF in their composites were very necessary to achieve the low volume resistivity at room temperature. The results were not surprising, because the CF-AgNWs was more easily to form conductive network in matrix. Thus they had an influence on the percolation threshold value. When the content was 2.5 wt %, the volume resistivity of the WPU/CF-AgNWs (1.90×10^4 Ω cm^{-1}) was lower by approximately three orders of magnitude than that of WPU/CF (4.19×10^7 Ω cm^{-1}). As Figure 10(a–e) showed, CF-AgNWs could contact with others partly in matrix with the increasing content of CF-AgNWs. When the content of CF-AgNWs was 2.5 wt %, the one-dimensional AgNWs with high aspect ratio could bridge the CF as shown in Figure 10(f). Moreover, the highly conductive AgNWs grown on the CF surface could improve the electrons transformation and decrease the charge transfer resistance of the CF. Therefore, the transportation of electrons was much easier and the volume resistivity of WPU/CF-AgNWs was lower than that of WPU/CF.

Dielectric Properties

As Figure 11 showed, all composites showed similar dielectric stability on frequency, and their dielectric constant and dielectric loss increased with the increase content of filler. Compared to the pristine CF [Figure 11(a)], CF-AgNWs led to more improvement in the dielectric constant of WPU, as Figure 11(c) showed. With the same loading of filler(2.5 wt %), the dielectric constant of WPU/CF composite increased from 6.3 for pure WPU to 11.3, while it increased to 15.24 for WPU/CF-AgNWs composite. Also, the addition of CF and CF-AgNWs influenced the dielectric loss of WPU. Compared to the pristine CF [Figure 11(b)], CF-AgNWs led to more improvement in the dielectric loss of WPU. As shown in Figure 11(d), when the content of filler was 2.5 wt %, the dielectric loss of the WPU/CF-AgNWs

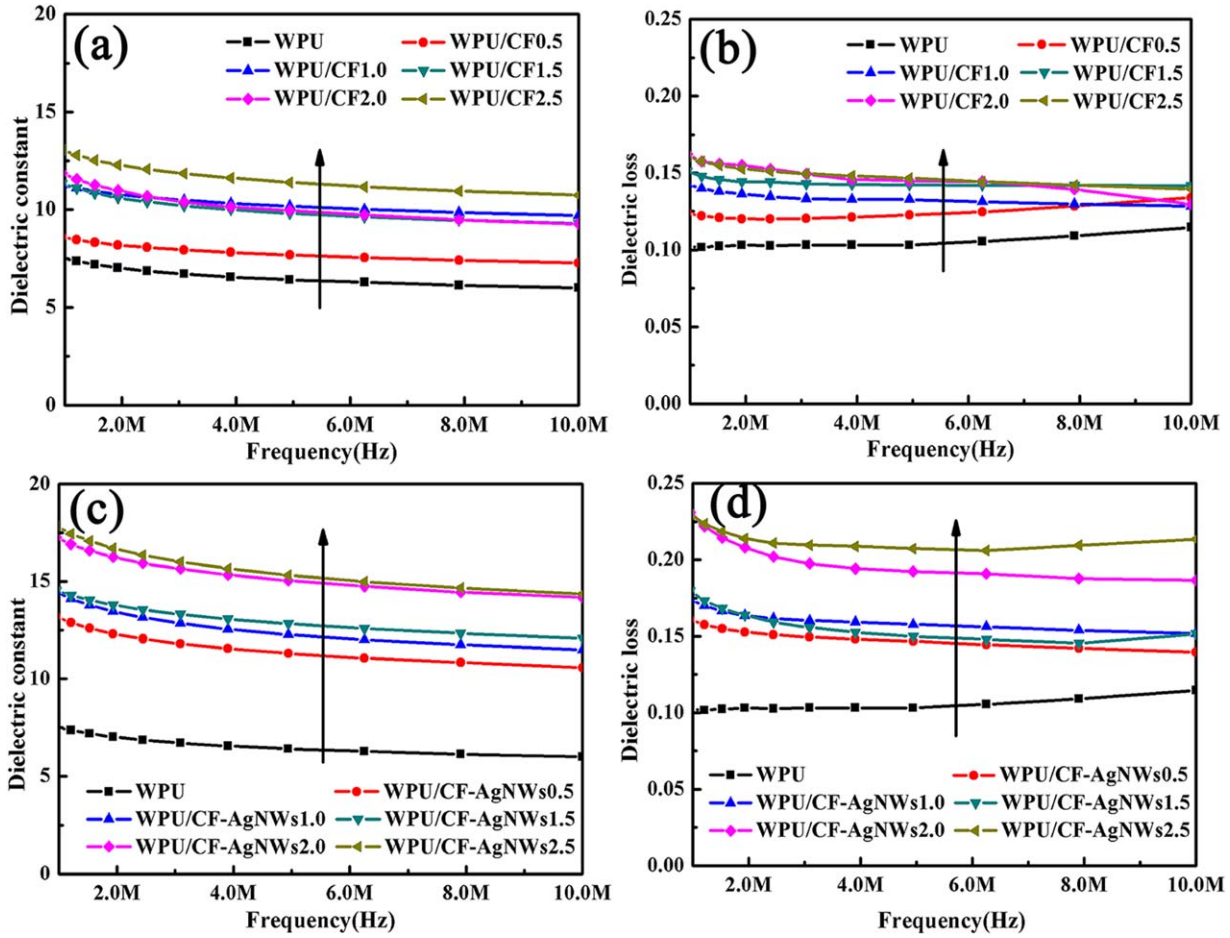

Figure 11. Dielectric constant and loss of WPU/CF composite (a and b) and WPU/CF-AgNWs composite (c and d) with different filler contents. [Color figure can be viewed in the online issue, which is available at wileyonlinelibrary.com.]

was improved to 0.21, which were 40.8% higher than that of WPU/CF. It was due to the AgNWs grown on CF improved the dipole moment, resulting in improved dielectric properties of WPU.

Table II. Tensile Properties of Samples in this Study

Sample	Breaking strength (MPa)	Elongation at break (%)
WPU	0.81 ± 0.038	237 ± 7.31
WPU/CF0.5	0.86 ± 0.044	225 ± 5.52
WPU/CF1.0	0.88 ± 0.040	191 ± 5.76
WPU/CF1.5	0.99 ± 0.076	174 ± 3.96
WPU/CF2.0	0.84 ± 0.038	197 ± 4.32
WPU/CF2.5	0.89 ± 0.035	156 ± 6.02
WPU/CF-AgNWs0.5	0.87 ± 0.027	191 ± 3.65
WPU/CF-AgNWs1.0	1.08 ± 0.037	208 ± 5.12
WPU/CF-AgNWs1.5	0.92 ± 0.023	151 ± 5.89
WPU/CF-AgNWs2.0	0.89 ± 0.038	141 ± 6.60
WPU/CF-AgNWs2.5	0.93 ± 0.041	140 ± 7.29

Mechanical Properties

Mechanical property was one of the most important properties of the composites. As Table II showed, for the net WPU, the breaking strength and elongation at break were 0.81 MPa and 237%, respectively. After the addition of pristine CF, the mechanical properties of WPU increased. When the CF content was 1.5 wt %, breaking strength of the WPU/CF composite reached the maximum. It increased from 0.81 to 0.99 MPa (an increase of 22.2%), which was because that the CF in polymer matrices play a vital role in load transfer. However, the breaking strength of the composite was decreased when the CF content continued to increase. But it was still higher than that of net WPU. This could be due to the uneven dispersion and regional agglomeration of the CF in the composite, which limited the efficiency of reinforcement.

As compared to the pristine CF, CF-AgNWs leads to more pronounced improvement in the mechanical properties of WPU. When the content was 1.0 wt %, the resultant composites exhibit 33.3% increases in breaking strength (compared to pure WPU). And the breaking strength reached the maximum value (1.08 MPa), which were higher than those of the WPU/CF composites. This probably due to the high aspect ratio of AgNWs

which could increase the surface area of CF. It was well known that the interface plays an important role in reinforcing the composites by effectively transferring the stress between the reinforcement and the matrix.[57] Thus compared with pristine CF, there were more interface between WPU and CF-AgNWs fillers. And AgNWs on the CF surface provided mechanical interlocking and it could be embedded in polymer. That resulted in higher breaking strength for WPU composite filled with CF-AgNWs. However, further increase of the CF-AgNWs content didn't lead to the increase of breaking strength of the composite. Such a phenomenon was also observed in other reports.[58] It could be due to the agglomeration of CF-AgNWs. The agglomeration would reduce the amount of interphase region and creates stress concentration sites which initiate failure.

As shown in Table II, the elongation values of the WPU/CF-AgNWs composite and the WPU/CF composite were all lower than that of net WPU. Moreover, the elongation value of WPU/CF-AgNWs composite was higher than that of WPU/CF composite. The results indicated that strong interfacial interaction between CF-AgNWs and WPU, which leaded to difficult deformation of the composites under the tensile loading.

CONCLUSION

In summary, AgNWs was grown on cysteamine-treated CF by a facile polyol method. The structure and formation mechanism of CF-AgNWs were studied. The CF-AgNWs was filled into the WPU to improve the materials' electrical property. Based on the experimental results, the following conclusions can be drawn:

1. It was found that appropriate conditions for the growth of AgNWs on CF were $AgNO_3$ concentration of 1.5 m*M*, reaction temperature of 160°C and reaction time of 120 min.
2. The impurities on CF were removed with acetone. Cysteamine was reacted with epoxy group of CF so that the surface of CF possessed thiol group. The formation of AgNWs on CF might be governed by formation of nucleation centers, growth of nucleus and growth of AgNWs. Reduced silver nanoparticles were attached to the CF via the silver bonding to sulfur (Ag-S). In the presence of PVP, silver nanoparticles served as seeds for growth of AgNWs, and then the CF-AgNWs was produced.
3. The volume resistivity of WPU/CF-AgNWs composite was decreased with the increase of filler contents. It was found that the WPU/CF-AgNWs composite presented a lower percolation threshold than WPU/CF composite. When the content was 2.5 wt %, the volume resistivity of the WPU/CF-AgNWs (1.90×10^4 Ω cm^{-1}) was lower by approximately three orders of magnitude than that of WPU/CF (4.19×10^7 Ω cm^{-1}).
4. The dielectric constant and dielectric loss of WPU/CF-AgNWs composite were increased with the increase of filler contents. When the content was 2.5 wt %, the dielectric constant and dielectric loss of the WPU/CF-AgNWs were improved to 15.24 and 0.21, which were 34.5 and 40.8% higher than that of WPU/CF.
5. The addition of CF-AgNWs improved the mechanical properties of WPU. When the content of CF-AgNWs was 1.0 wt %, the resultant composites exhibited 33.3% increases in breaking strength (compared to pure WPU).

The WPU/CF-AgNWs was regarded as promising materials for use in electromagnetic shielding. Furthermore, the concept of using CF-AgNWs as fillers in this study will also be applicable to a wide range of other polymer composites for use in electromagnetic shielding. The research provided a theoretical basis for our further study.

REFERENCES

1. Hernandez, E. A.; Posada, B.; Irizarry, R.; Castro, M. E. *J. Phys. Chem. B* **2005**, *109*, 7251.
2. Zhang, P.; Shao, C.; Zhang, Z.; Zhang, M.; Mu, J.; Guo, Z.; Liu, Y. *Nanoscale* **2011**, *3*, 3357.
3. Huang, Y. L.; Baji, A.; Tien, H. W.; Yang, Y. K.; Yang, S. Y.; Wu, S. Y.; Ma, C. C. M.; Lin, H. Y.; Mai, Y. W.; Wang, N. H. *Carbon* **2012**, *50*, 3473.
4. Shi, L.; Yang, J.; Yang, T.; Hanxun, Q.; Li, J.; Zheng, Q. *Rsc. Adv.* **2014**, *4*, 43270.
5. Jiang, Y.; Lu, Y.; Zhang, L.; Liu, L.; Dai, Y.; Wang, W. *J. Nanopart. Res.* **2012**, *14*, 1.
6. Wang, J.; Jiu, J.; Araki, T.; Nogi, M.; Sugahara, T.; Nagao, S.; Koga, H.; He., P.; Suganuma, K. *Nano-Micro. Lett.* **2015**, *7*, 51.
7. Hu, M.; Gao, J.; Dong, Y.; Yang, S.; Li, R. K. Y. *Rsc. Adv.* **2012**, *2*, 2055.
8. An, C.; Wang, J.; Wang, S.; Zhang, Q.; Yang, M.; Zhan, J. *CrystEngComm* **2012**, *14*, 5886.
9. Yu, D.; Yao, J.; Qiu, L.; Wu, Y.; Li, L.; Feng, Y.; Liu, Q.; Li, D.; Wang, H. *Rsc. Adv.* **2012**, *3*, 11552.
10. Chen, L.; Chabu, J.; Jin, M.; Xiao, R. *J. Rsc. Adv.* **2013**, *3*, 26102.
11. Tang, C.; Sun, W.; Yan, W. *Rsc. Adv.* **2014**, *4*, 523.
12. Samantara, A. K.; Mishra, D. K.; Suryawanshi, S. R.; More, M. A.; Thapa, R.; Late, D. J.; Jena, B. K.; Rout, C. S. *Rsc. Adv.* **2015**, *5*, 41887.
13. Yun, Y. S.; Kim, D. H.; Kim, B.; Park, H. H.; Jin, H. *J. Synth. Met.* **2012**, *162*, 1364.
14. Tokuno, T.; Nogi, M.; Jiu, J.; Suganuma, K. *Nanoscale Res. Lett.* **2012**, *7*, 1.
15. Liu, Y.; Chang, Q.; Huang, L. *J. Mater. Chem. C* **2013**, *1*, 2970.
16. Xu, S.; Man, B.; Jiang, S.; Liu, M.; Yang, C.; Chen, C.; Zhang, C. *CrystEngComm* **2014**, *16*, 3532.
17. Li, N.; Huang, G. W.; Shen, X. J.; Xiao, H. M.; Fu, S. Y. *J. Mater. Chem. C* **2013**, *1*, 4879.
18. Choi, H. O.; Kim, D. W.; Kim, S. J.; Cho, K. M.; Jung, H. T. *J. Mater. Chem. C* **2014**, *2*, 5902.
19. Kim, D.; Zhu, L.; Jeong, D. J.; Chun, K.; Bang, Y. Y.; Kim, S. R.; Kim, J. H.; Oh, S. K. *Carbon* **2013**, *63*, 530.

20. Qin, H.; Jiang, L.; He, Y.; Liu, J.; Cao, K.; Wang, J.; He, Y.; Ni, H.; Chi, H.; Ji, Z. *J. Mater. Chem. A* **2013**, *1*, 15323.
21. Gao, C.; Li, W.; Jin, Y. Z.; Kong, H. *Nanotechnology* **2006**, *17*, 2882.
22. Tseng, C. H.; Chen, C. Y. *Nanotechnology* **2008**, *19*, 035606.
23. Hsiao, S. T.; Tien, H. W.; Liao, W. H.; Wang, Y. S.; Li, S. M.; Ma, C. C. M.; Yu, Y. H.; Chuang, W. P. *J. Mater. Chem. C* **2014**, *2*, 7284.
24. Tien, H. W.; Hsiao, S. T.; Liao, W. H.; Yu, Y. H.; Lin, F. C.; Wang, Y. S.; Li, S. M.; Ma, C. C. M. *Carbon* **2013**, *58*, 198.
25. Cui, L.; Du, Z.; Zou, W.; Li, H.; Zhang, C. *Rsc. Adv.* **2014**, *4*, 27591.
26. Jun, Z.; Peng, T.; Sen, W.; Xu, J. *Appl. Surf. Sci.* **2009**, *255*, 4916.
27. Liao, Q.; Mohr, M.; Zhang, X.; Zhang, Z.; Zhang, Y.; Fecht, H. *J. Nanoscale* **2013**, *5*, 12350.
28. Koerner, H.; Liu, W.; Alexander, M.; Mirau, P.; Dowty, H.; Vaia, R. A. *Polymer* **2005**, *46*, 4405.
29. Kwon, J.; Kim, H. *J. Polym. Sci. Polym. Chem.* **2005**, *43*, 3973.
30. Lu, X.; Xu, G.; Hofstra, P. G.; Bajcar, R. C. *J. Polym. Sci. Polym. Phys.* **1998**, *36*, 2259.
31. Ma, J.; Zhan, M. *Rsc. Adv.* **2014**, *4*, 21060.
32. Cai, M.; Ho, M.; Pemberton, J. E. *Langmuir* **2000**, *16*, 3446.
33. Shen, Z. Y.; Li, L. Y.; Li, Y.; Wang, C. C. *J. Colloid. Interface Sci.* **2011**, *354*, 196.
34. Dai, Z.; Shi, F.; Zhang, B.; Li, M.; Zhang, Z. *Appl. Surf. Sci.* **2011**, *257*, 6980.
35. Wu, Q.; Li, M.; Gu, Y.; Wang, S.; Wang, X.; Zhang, Z. *J. Appl. Polym. Sci.* **2015**, *132*, 41917.
36. Pandey, S.; Mewada, A.; Thakur, M.; Tank, A.; Sharon, M. *Rsc. Adv.* **2013**, *3*, 26290.
37. Niu, H. L.; Wu, X. H.; Qiu, M.; Gao, Y. H.; Song, J. M.; Mao, C. J.; Zhang, S. Y. *J. Mater. Res.* **2011**, *26*, 2780.
38. Karir, T.; Sarma, H. D.; Samuel, G.; Hassan, P. A.; Padmanabhan, D.; Venkatesh, M. *J. Appl. Polym. Sci.* **2013**, *130*, 860.
39. Kumar, S.; Ghosh, S.; Munichandraiah, N.; Vasan, H. V. *Nanotechnology* **2013**, *24*, 235101.
40. Feng, L.; Wang, C.; Ma, Z.; Lü, C. *Dyes Pigm.* **2013**, *97*, 84.
41. Ge, H.; Ma, X.; Liu, H. *J. Appl. Polym. Sci.* **2015**, *132*.
42. Cao, X. H.; Zhang, M. M.; Liu, Y. H.; Nie, W. B. *J. Electrochem. Soc.* **2012**, *159*, B850.
43. Bertin, A.; Schlaad, H. *Chem. Mater.* **2009**, *21*, 5698.
44. Bayram, S.; Zahr, O. K.; Blum, A. S. *Rsc. Adv.* **2015**, *5*, 6553.
45. Chen, H.; Wang, N.; Di, J.; Zhao, Y.; Song, Y.; Jiang, L. *Langmuir* **2010**, *26*, 11291.
46. Zhao, P.; Zhang, J.; Zhu, Y.; Yang, X.; Jiang, X.; Yuan, Y.; Liu, C.; Li, C. *J. Mater. Chem. B* **2014**, *2*, 8372.
47. Kudelski, A.; Hill, W. *Langmuir* **1999**, *15*, 3162.
48. Zhang, Z. Z.; Song, H. J.; Men, X. H.; Luo, Z. Z. *Wear* **2008**, *7*, 599.
49. Ma, J.; Zhan, M.; Wang, K. *ACS. Appl. Mater. Interfaces* **2015**, *7*, 563.
50. Lee, S. H.; Teng, C. C.; Ma, C. C. M.; Wang, I. *J. Colloid. Interface Sci.* **2011**, *364*, 1.
51. Ma, J.; Wang, K.; Zhan, M. *ACS. Appl. Mater. Interfaces* **2015**, *7*, 16027.
52. Mu, J.; Chen, B.; Guo, Z.; Zhang, M.; Zhang, Z.; Zhang, P.; Shao, C.; Liu, Y. *Nanoscale* **2011**, *3*, 5034.
53. Zhang, Z.; Wang, Z.; He, S.; Wang, C.; Jin, M.; Yin, Y. *Chem. Sci.* **2015**, *6*, 5197.
54. Akhavan, O.; Abdolahad, M.; Abdi, Y.; Mohajerzadeh, C. *J. Mater. Chem.* **2011**, *21*, 387.
55. Liu, X.; Du, H.; Sun, X. W.; Liu, B.; Zhao, D.; Sun, H. *Cryst. Eng. Commun.* **2012**, *14*, 2886.
56. Liu, W.; Lu, C.; Wang, X.; Tay, R. Y.; Tay, B. K. *ACS Nano* **2015**, *9*, 1528.
57. Zeng, X.; Yu, S.; Ye, L.; Li, M.; Pan, Z.; Sun, R.; Xu, J. *J. Mater. Chem. C* **2015**, *3*, 187.
58. Xiong, J.; Zheng, Z.; Qin, X.; Li, M.; Li, H.; Wang, X. *Carbon* **2006**, *44*, 2701.